Aluminum oxide barrier layers on polymer web

C. F. Struller[a, b, 1], P. J. Kelly[a], N. J. Copeland[b] and C. M. Liauw[c]

[a]Surface Engineering Group, Manchester Metropolitan University, Manchester, M1 5GD, UK
[b]Bobst Manchester Ltd., Pilsworth Road, Heywood, Lancashire OL10 2TL, UK
[c]School of Engineering, Manchester Metropolitan University, Manchester, M1 5GD, UK

ABSTRACT

Aluminum oxide barrier layers have been deposited onto BOPP and PET film substrates via reactive evaporation of aluminum using an industrial 'boat-type' roll-to-roll metallizer. The effects of parameters such as treatment, surface chemistry, film additives, and surface roughness and topography on barrier levels have been investigated. Additionally, coating adhesion, thickness and surface energy have been assessed. Whilst good adhesion was achieved regardless of barrier properties, the plain film surface characteristics and coating nucleation, growth and structure appeared to be the governing factors for barrier performance.

INTRODUCTION

Thermal evaporation of thin aluminum layers onto commodity polymer films via roll-to-roll vacuum web coating represents a common technique in the field of food packaging materials and other applications. In regards to foodstuffs, the packaging material needs to meet certain standards in order to be able to preserve the food products and ensure a long shelf life. Thus, barrier properties against moisture and oxygen ingress are key properties for successful food packaging. Transparent barrier coatings on polymer films not only provide barrier against moisture and oxygen, but also offer further advantages, such as product visibility and microwaveability. Traditionally, products such as ethylene vinyl alcohol copolymer (EVOH) co-extruded barrier layer films and polyvinylidene chloride (PVdC) atmospheric coated polymer films tend to dominate the clear barrier flexible packaging market [1]. However, EVOH is moisture sensitive and loses its barrier at high humidity [2], whilst PVdC coated polymer films have fallen into disrepute due to the possible release of dioxins upon incineration [3]. Furthermore, these conventional polymer based barrier layers have thicknesses of several microns, while vacuum deposited barrier layers only require thicknesses in the nanometer range. During the last two decades, a development towards the production of transparent ceramic barrier layers, i.e. aluminum oxide (AlO_x), using industrial 'boat-type' roll-to-roll vacuum web coaters with high throughput has taken place [4-9]. Therefore, the standard aluminum metallization process is modified by introducing oxygen into the evaporation zone, thus resulting in the deposition of a transparent aluminum oxide layer. Using this well established process gives the unique possibility to produce transparent barrier films at low cost via standard high speed coating equipment.

Whilst the process produces consistent barrier performance with reactively evaporated aluminum oxide on polyethylene terephthalate (PET), biaxially oriented polypropylene (BOPP) films, which offer cost advantages over PET, have proven to be a more difficult substrate. Excluding coating densification techniques, the barrier levels of aluminum oxide coated BOPP greatly depend on the plain film surface

[1]Carolin.struller@stu.mmu.ac.uk, Manchester Metropolitan University, John Dalton Building, Chester Street, Manchester, M1 5GD, United Kingdom, Tel: +44 (0) 161 247 4694, Fax: +44 (0) 161 247 4693

and thus the growth conditions for the depositing thin film, both of which can vary to a large extent. Therefore, this paper characterizes plain film surface properties, such as surface energy, roughness and topography. Furthermore, coating to substrate adhesion, aluminum oxide thickness and coating surface energy were also investigated.

EXPERIMENTAL

Various packaging grade BOPP (corona treated at manufacture's site) and PET base films, as well as a BOPP film with a special polymer as skin layer, have been coated using a General Vacuum Equipment (now Bobst Manchester) K4000 vacuum metallizer (with an AlO_x coating system installed). The K4000 roll-to-roll metallizer can handle webs up to 2450 mm wide. Films were coated at web speeds up to 800 m/min. Additionally, in-line plasma pre- and post-treatments were performed using a plasma source with magnetically enhanced water cooled electrodes. For the purpose of the trials conducted for this study, other than plasma treatment conditions all coating parameters were kept constant.

Oxygen and water vapor transmission rates (OTR/WVTR) were analyzed according to ASTM F 1927 and F 1249 using a Mocon Oxtran 2/20 and Systech Illinois 8001 for oxygen permeation and a Mocon Permatran-W 33/3 and Systech Illinois 7001 for water vapor permeation. Test conditions for OTR were 23 °C and 50 % relative humidity (RH), while WVTR is stated for 38 °C and a gradient of 90 % RH.

Differential interference contrast (DIC) microscopy images were obtained using a Zeiss Axio Imager.M2m optical microscope.

Furthermore, a Zeiss Supra 40VP field emission gun scanning electron microscope (SEM) was used to acquire images of the plain film and aluminum oxide coated surfaces. Coatings were examined with a 0.4/0.5 kV acceleration voltage and without applying any conductive layer to avoid masking surface detail.

The plain film and coating surfaces were additionally analyzed with a WiTec alpha500 and a Veeco DI CP II atomic force microscope (AFM). Pulsed force mode and tapping mode, respectively, were used to acquire roughness data and topography images. All images were corrected by line-wise leveling.

Measurement of coating adhesion was performed using a peel test as described in [10, 11]. This industrial based test is normally applied to assess the adhesion of aluminum metallized films.

Infrared spectra were recorded with a Thermo Scientific Nicolet 380 Fourier transform infrared (FT-IR) spectrometer using a single bounce diamond attenuated total reflectance (ATR) accessory.

The surface energy was investigated by means of contact angle measurement via the sessile drop method. A Krüss MobileDrop contact angle measuring system was used. Based on the measured contact angles of three test fluids (water, diiodomethane and ethylene glycol), the surface energies were calculated according to the Owens-Wendt-Rabel-Kaelble approach [12-14]. Sample swatches were stored under ambient conditions.

The surface contamination on the AlO_x coated BOPP films was examined using X-ray photoelectron spectroscopy (XPS) via a Thermo Scientific Theta Probe XPS instrument with an electron take-off angle of 37° (probing depth 5 to 6 nm).

A FEI Tecnai 12 Biotwin transmission electron microscope (TEM) was used to acquire images of the AlO_x layer for coating thickness evaluation.

RESULTS AND DISCUSSION

A. Barrier performance

Table 1 summarizes the barrier results for the different AlO_x coated BOPP films and different plasma treatment variations (marked PRE and POST as appropriate). Following extensive coating trials on various BOPP base substrates, it was decided to limit the results presented and the film choices were consolidated to the following:

- BOPP A – poor performing polymer
- BOPP B – standard performing polymer
- BOPP C – standard performing polymer with improved oxygen barrier
- BOPP D – special polymer skin layer

For comparison, the table also contains barrier levels obtained on standard grade PET film, the plain film barrier performances and barrier improvement factors (BIF). As can be seen, the OTR and WVTR measured for AlO_x coated PET were both around 0.5 $cm^3/(m^2\ d)$ and 0.5 $g/(m^2\ d)$, respectively.

Table 1 – Barrier performance of plain and AlO_x coated films

Film/ Thickness	**Plasma treatment**	**OTR**		**WVTR**	
		$cm^3/(m^2\ d)$	**BIF**	**$g/(m^2\ d)$**	**BIF**
BOPP A	Plain film	≈ 1600	**-**	≈ 4	**-**
30 µm	PRE	205.24 ± 27.37	**7**	3.43 ± 0.35	**1.1**
	PRE + POST	244.00 ± 7.07	**7**	3.98 ± 0.30	**1**
BOPP B	Plain film	≈ 2700	**-**	≈ 7	**-**
15 µm	PRE + POST	85.56 ± 16.80	**32**	5.89 ± 0.18	**1.2**
BOPP C	Plain film	≈ 2400	**-**	≈ 6	**-**
20 µm	No	47.00 ± 5.35	**51**	5.89 ± 0.23	**1**
	PRE	35.33 ± 3.05	**68**	6.08 ± 0.17	**1**
	PRE + POST	25.35 ± 1.38	**95**	4.73 ± 0.07	**1.3**
BOPP D	Plain film	≈ 500	**-**	≈ 4.5	**-**
18 µm	No	0.89 ± 0.01	**562**	2.18 ± 0.07	**2**
	PRE	0.83 ± 0.30	**602**	0.62 ± 0.07	**7**
	PRE + POST	0.60 ± 0.14	**833**	0.55 ± 0.25	**8**
PET	Plain film	≈ 120	**-**	≈ 40	**-**
12 µm	PRE + POST	0.54 ± 0.05	**185**	0.56 ± 0.03	**80**

With the AlO_x system, values below 1 $cm^3/(m^2\ d)$ and 1 $g/(m^2\ d)$ are reliably achieved on standard packaging grade PET film without the need for sophisticated and expensive densification processes. However, for the AlO_x coated BOPP films, the barrier performance strongly depends on the base material itself. BOPP, in contrast to PET, is a non-polar polymer with a completely different surface chemistry, which has a large impact on coating nucleation and growth. The barrier results for BOPP A, for example, were fairly inconsistent and none of the trials performed resulted in a clear improvement of the oxygen barrier down to levels below 100 $cm^3/(m^2\ d)$, i.e. comparable to aluminum metallized BOPP. On BOPP C, by contrast, very good oxygen barrier performance was obtained. The OTR values for AlO_x coated BOPP C clearly revealed an improvement in barrier levels through the additional application

of plasma pre- and post-treatment. Pre-treatment improves barrier by chemical modification of the plain film surface, which enhances coating nucleation/growth conditions and structure [15]. The bombardment of the coating during post-treatment can result in a densification of the outermost atomic layers of the coating, which may protect the AlO_x layer and reduce oxygen permeation. AlO_x coated BOPP B also exhibited oxygen barrier levels comparable to metallized BOPP, however, not to the level achieved for BOPP C. These results show that whether a good barrier performance on BOPP is obtained or not is very much base film dependent, which clearly makes this a film and not a process related issue based on the optimized process used. Possible reasons for the barrier differences between the BOPP films A, B and C will be discussed in the next sections with the results of the SEM and AFM investigations. Despite the good oxygen barrier obtained for BOPP film type C, the moisture barrier achieved was not comparable to metallized BOPP, i.e., the barrier improvement factor was negligible. This fact confirms that oxygen and moisture permeation through inorganic barrier layers are dominated by different mechanisms [16-19]. However, plain BOPP film already has an inherently good water barrier. In the case of the modified surface BOPP film, BOPP D, which had a special high surface energy polymer skin layer in order to enhance barrier performance after coating, remarkable barrier improvement for both OTR and WVTR could be obtained by applying the AlO_x layer (refer to *Table 1*). Furthermore, this data also shows the importance of in-line plasma pre-treatment for obtaining a water barrier performance of less than 1 g/(m² d) for the AlO_x coated film.

B. Surface topography

The plain BOPP films and AlO_x coated samples have been investigated further by DIC light microscopy, SEM and AFM analysis. Optical DIC microscopy gives the possibility of obtaining information about the topography in a three-dimensional impression of the specimen surface and also gathering information about the size and density distribution of the antiblock particles present on the film surface (refer to *Figure 1*).

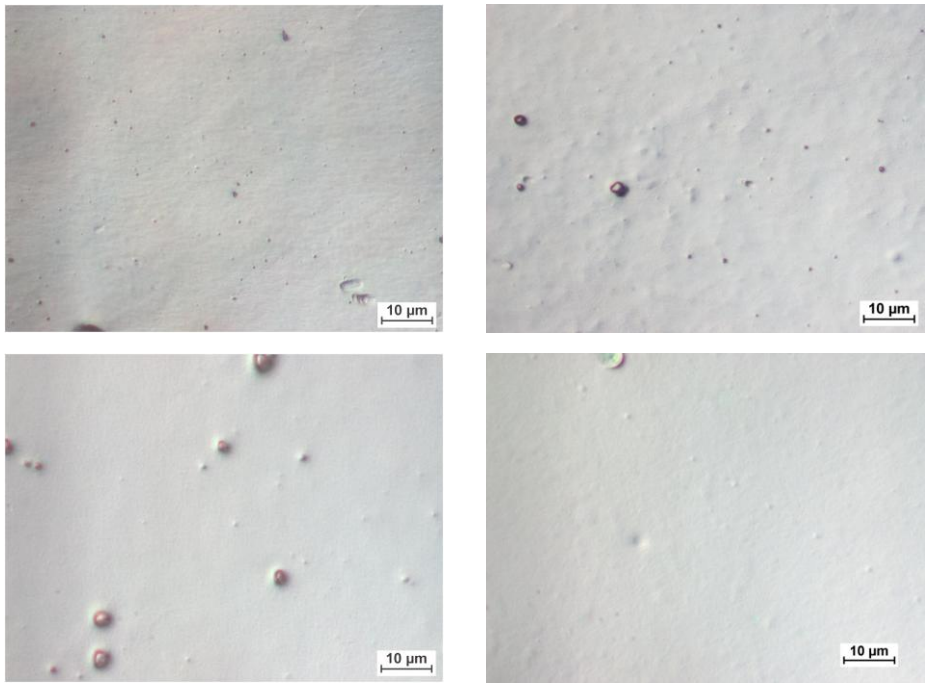

Figure 1 – DIC images of plain film – top left BOPP A, top right BOPP B, bottom left BOPP C, bottom right BOPP D

Antiblock particles, commonly consisting of silica, are additives incorporated into the film in order to ease film handling during processing by modifying surface roughness and acting as spacers between adjacent surfaces in the rolls of film [20]. Whilst BOPP A and B showed a large number of small (sub µm size) antiblock particles, BOPP C featured fewer but substantially larger antiblock particles (diameter > 1 µm). In contrast to all these standard BOPP films, BOPP D does not contain any antiblock particles. The SEM images of the plain BOPP film surfaces also showed antiblock particles of various sizes protruding from the film surface (see *Figure 2*). Once again, BOPP A and B revealed a larger amount of sub µm size antiblock particles in the SEM investigation in comparison with BOPP C. All three BOPP films exhibited a grainy surface structure ('orange-peel'), however, with major individual differences. On BOPP B the grains were a lot larger than on BOPP A and C, whereas for BOPP A an additional texture with a diagonal orientation appeared to overlay the grainy structure. Furthermore, a key difference between BOPP A and B/C was seen, in that BOPP A featured 'dimples' (small craters) with diameters of 100 nm to several 100 nm (measured via AFM). The origin of these defects is unknown, but will be further investigated. The damage seen on BOPP A (*Figure 2*, left image, center) has been created by an antiblock particle dislocating from the film surface.

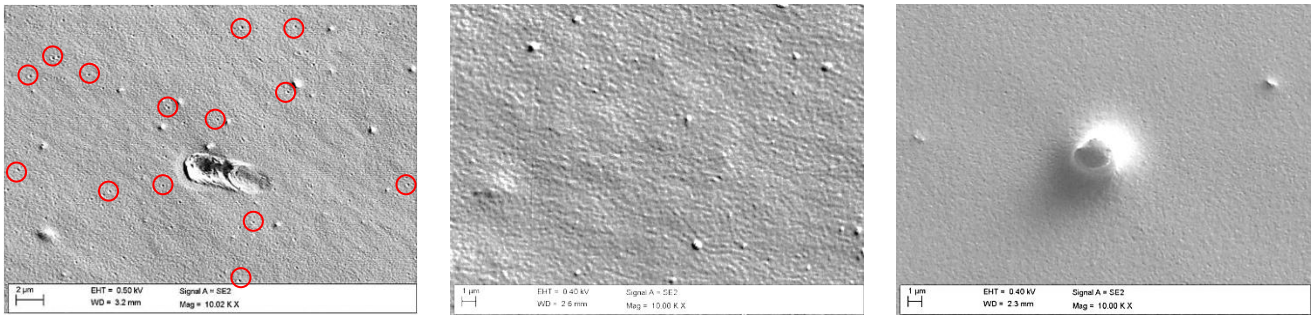

Figure 2 – SEM images of plain film surfaces (10 000x magnification) – left to right: BOPP A ('dimples' marked by circles), BOPP B, BOPP C

The PET film surface (no images shown) was visibly different to the BOPP films and revealed a large surface coverage of antiblock particles; nevertheless, these particles gave the appearance of being more incorporated into the PET film surface than was the case for the BOPP films. In all cases, the AlO_x coated film surfaces looked very similar to the plain film surfaces, with the AlO_x coating reproducing the plain film surface topography as shown in *Figure 3*.

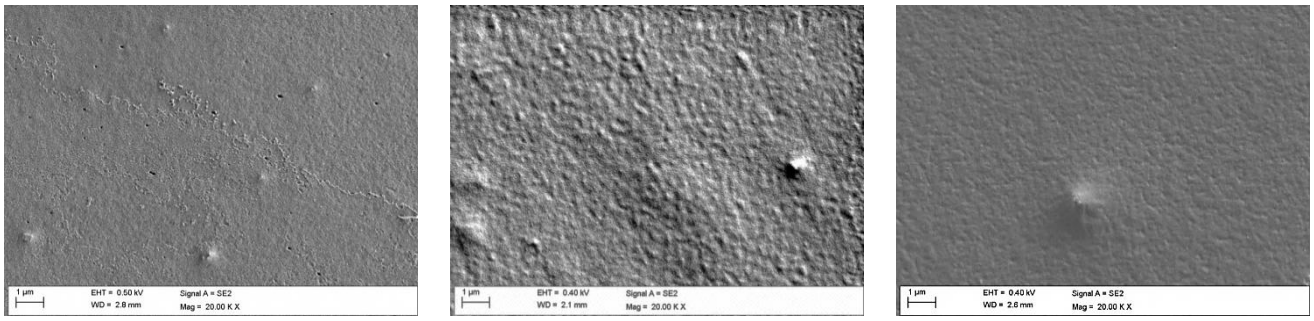

Figure 3 – SEM images of AlO_x coated film surfaces (20 000x magnification) – from left to right: BOPP A, BOPP B, BOPP C

However, on comparing the SEM images of AlO_x coated BOPP A with B and C, major differences could again be seen. Whilst on BOPP B and C the AlO_x surface had a very 'regular' surface appearance, the coating on BOPP A exhibited pores and what appeared to be variations in coating thickness. AFM analysis of the plain film and AlO_x coated surfaces confirmed the results of the SEM investigations and revealed the same 'grainy' structures and other surface features (refer to *Figure 4* for AFM images of plain BOPP films). For example, pores were again detected by the AFM examinations of AlO_x coated BOPP film A. As pores could neither be found on AlO_x coated BOPP B or C, it is assumed that these pores are major pathways for oxygen molecules, which result in the high OTR values for AlO_x coated BOPP A (see *Table 1*). AFM and SEM analysis already showed the presence of dimples in the plain film surface of BOPP A, which were of similar dimensions to the pores in the AlO_x coating and, therefore, may have caused these pores. Clearly, the plain film surface seems to be of great importance in regard to the barrier levels of the AlO_x coated film, and differences in the surfaces of the plain BOPP films seem to account for the large differences measured in OTR for BOPP A compared to B and C (for 'dimples' on BOPP A see left image of *Figure 2* and *Figure 4*).

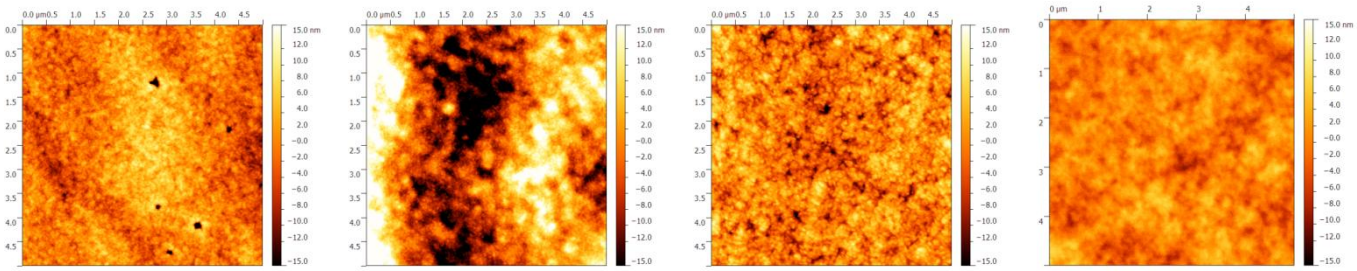

Figure 4 – 5 x 5 µm² AFM scans of plain film surfaces – from left to right: BOPP A, BOPP B, BOPP C, BOPP D

For AFM surface roughness evaluation, root mean square (RMS) and roughness average values were calculated from 5 x 5 μm^2 size scans and all scans were acquired in areas that did not include antiblock particles. Results of this investigation are summarized in *Table 2*.

Table 2 – Surface roughness of plain and AlO_x coated BOPP films (calculated from 5 x 5 µm² scans)

Film	Plasma treatment	Root mean square Nm	Roughness average nm
BOPP A	Plain film	4.1 ± 0.7	3.3 ± 0.5
	PRE	3.8 ± 0.5	3.0 ± 0.4
BOPP B	Plain film	5.7 ± 1.8	4.5 ± 1.5
	PRE	5.8 ± 0.9	4.6 ± 0.7
	PRE + POST	6.0 ± 0.7	4.8 ± 0.6
BOPP C	Plain film	4.1 ± 0.3	3.2 ± 0.2
	PRE	4.6 ± 0.2	3.6 ± 0.2
	PRE + POST	4.3 ± 0.3	3.4 ± 0.2
BOPP D	Plain film	2.8 ± 0.2	2.2 ± 0.1
	PRE	2.9 ± 0.2	2.3 ± 0.2
	PRE + POST	3.0 ± 0.2	2.4 ± 0.1
PET	Plain film	1.6 ± 0.2	1.2 ± 0.2
	PRE + POST	1.8 ± 0.3	1.4 ± 0.3

The lowest values were obtained on plain and AlO_x coated PET with average RMS values of 1.6/1.8 nm, whilst BOPP B gave the highest roughness values. Despite having a high surface roughness, BOPP B still showed acceptable OTR values, which supports the idea that nanoscale surface roughness of the plain film is not the main factor governing oxygen barrier performance after AlO_x coating. Plain BOPP A and C show approximately the same surface roughness (RMS 4.1 nm), but very different OTR values. Therefore, the roughness parameters give no indication about the defects ('dimples', pores) present on plain and AlO_x coated BOPP A. The roughness of BOPP D, the film with the modified skin layer, was lower than for all standard BOPP films, but higher than obtained for PET. The plain film roughness values measured for PET and BOPP are in good agreement with results obtained by Benmalek and Dunlop [21] and Deng et al. [22] despite small differences in the AFM scan size used for roughness evaluation. Additionally, the AFM investigation shows that for each film type the plain film and AlO_x coating roughness are approximately in the same range as found by other researchers [22-24].

C. Surface chemistry

The plain standard grade BOPP films have been further characterized in terms of surface chemistry via contact angle measurement for surface energy determination. As can be seen from the results presented in *Table 3*, the surface energy did not reveal any significant differences between the three films, but gave standard levels for corona treated BOPP film. Nevertheless, in order to further characterize the films and detect possible differences, the exact chemical composition of the plain BOPP films will additionally be studied using XPS analysis.

Table 3 – Surface energy results for plain BOPP films

Film	Surface energy mN/m		
	Polar	Dispersive	Total
BOPP A	8.9 ± 0.6	29.1 ± 0.4	38.0 ± 0.4
BOPP B	7.8 ± 0.6	28.6 ± 0.3	36.4 ± 0.4
BOPP C	7.9 ± 0.2	28.7 ± 0.1	36.6 ± 0.2

D. Coating thickness

In order to determine the thickness of the reactively evaporated AlO_x layers, film samples were embedded in an epoxy resin, cross-sectioned with an ultramicrotome and subsequently examined using TEM. *Figure 5* shows TEM cross section images at two different magnification levels for AlO_x coated BOPP. For standard BOPP films, TEM revealed the typical three layer structure with a core layer surrounded by a skin layer on each side (left image of *Figure 5* shows one skin layer only). In all cases, the thickness of the AlO_x barrier layer was determined to be between 9 and 11 nm (refer to *Figure 5*, right image), which is approximately only one fourth of the thickness of an aluminum layer on a standard metallized film with an optical density of 2.5 [25].

The damage seen on the AlO_x coating (inconsistent layer) in the left image of *Figure 5* is due to the sample preparation process, i.e. the compression during microtoming, and the different elastic properties of the BOPP polymer, the embedding medium and the brittle AlO_x coating.

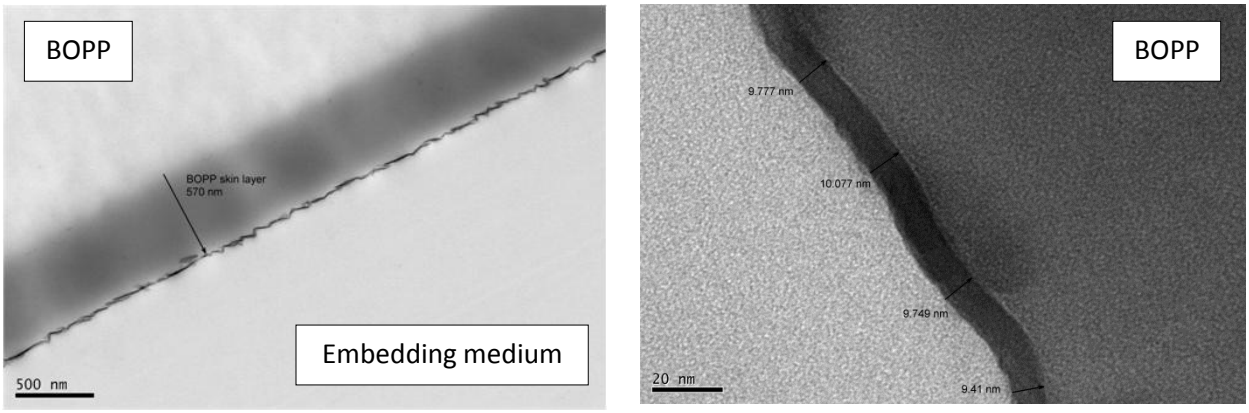

Figure 5 – TEM thickness measurements on AlO_x coated BOPP film

E. Coating adhesion

Since vacuum coated films are further converted e.g. by laminating another polymer on top of the coating to protect the barrier layer, a good coating to substrate adhesion is an important criterion in preventing delamination during the final packaging application of the composite material. The adhesion of the reactively evaporated AlO_x coating to the BOPP films was assessed using a peel test normally used for the determination of the adhesion of aluminum coatings on polymer films. A major requirement for the validity of this test is the achievement of full coating removal. Our earlier investigations of AlO_x adhesion to BOPP films have shown that this peel test can be applied in the case of AlO_x coated polymer films. Full coating removal was possible and visible to the naked eye, despite the high transparency of the coated film (> 92 % light transmission). The peel strength values obtained are summarized in *Table 4*.

Table 4 – Peel-forces obtained for AlO_x coated BOPP films

Film	Plasma treatment	Peel force	
		N/(15 mm)	g/inch
BOPP A	PRE A	3.88 ± 0.09	669 ± 15
	PRE B	3.68 ± 0.14	635 ± 24
BOPP B	No	3.46 ± 0.08	597 ± 14
	PRE	3.51 ± 0.10	606 ± 18
	PRE + POST	3.50 ± 0.16	604 ± 27
BOPP C	No	5.05 ± 0.17	871 ± 29
	PRE	5.07 ± 0.12	875 ± 22
	PRE + POST	5.04 ± 0.14	869 ± 23
	Metallized, PRE	*1.09 ± 0.11*	*189 ± 19*

In all cases, very high peel strength values were obtained. These values far exceeded the adhesion values obtained for aluminum metallized standard packaging grade BOPP film (see peel strength obtained for metallized BOPP C, *Table 4*, bottom). The high peel strength values along with the apparent independence from the plasma pre-treatment suggests that, in addition to the AlO_x coating, polymeric material, such as the skin layer of the BOPP film, was also removed during the peel test. Consequently,

the EAA films which had been peeled-off were further analyzed by IR spectroscopy to see if the presence of polypropylene could be detected. ATR FT-IR has a wavelength dependent penetration depth of a few 100 nm to around 1 µm and consequently will not show small residues of polymeric origin on the peeled-off region. However, if a layer with a thickness of at least a few 100 nm of polymer is removed, this will be visible in the FT-IR spectra. For all three AlO_x coated BOPP film types, FT-IR confirmed that polymeric material, presumably the BOPP skin layer, was present on the peeled-off EAA film region, as the spectra revealed peaks unique to PP and EAA only. This shows that a cohesive failure occurred during the peel-tests, i.e. the locus of failure is not at the interphase between coating and substrate but within the substrate. Nevertheless, as the failure in a multilayer structure generally initiates at the weakest point of the system [26], it can be assumed the adhesion of the AlO_x coating to the BOPP film exceeds the values measured, which most likely represent the adhesion between the skin layer and the core layer of the BOPP film.

F. AlO_x surface energy

Further conversion of vacuum coated films, such as printing or laminating on top of the barrier layer, requires a high surface energy as this usually results in better wetting of inks or the adhesives used for lamination. Good wetting, in general, is the first step towards good adhesion. Therefore, the AlO_x coated BOPP films were analyzed at regular time intervals by contact angle measurement to investigate any change of surface energy that may take place over time. Surface energy results including standard deviations for AlO_x coated BOPP A, BOPP C and BOPP D are depicted as a function of time in *Figure 6*.

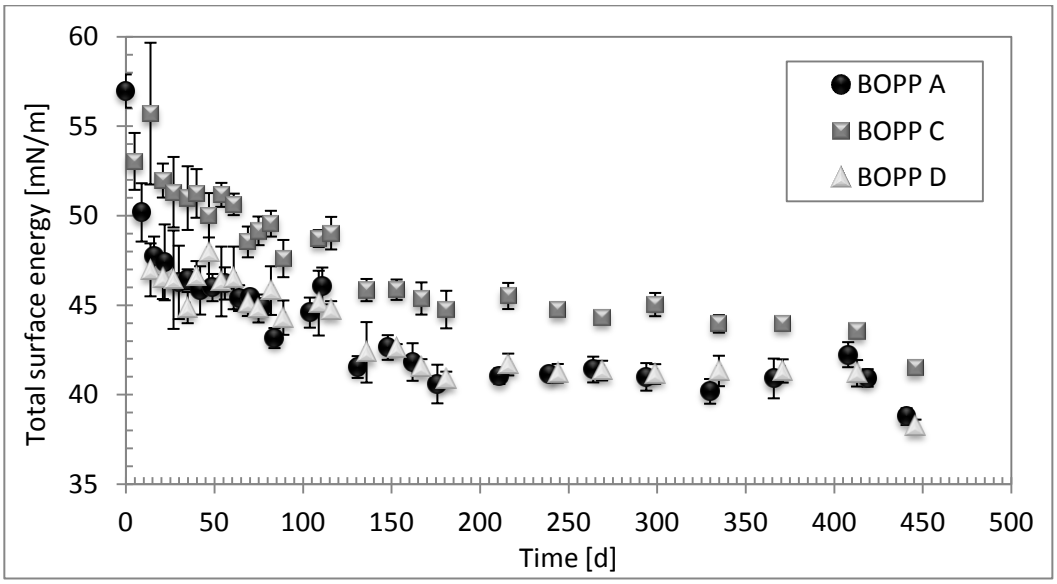

Figure 6 – Change of AlO_x surface energy with storage time

As can be seen for BOPP A, the surface energy decreases rapidly within the first 30 days from an initial value of 57.0 ± 0.9 mN/m and then decays further, however at a slower rate. After approximately 200 days this process slows down more. Nevertheless, there is still a measurable decline in surface energy even after 400 days. BOPP D behaves nearly identically to BOPP A and also BOPP B showed a similar behavior, though with the average AlO_x surface energy being somewhat higher than for the other

films. On separating the total surface energy into its polar and dispersive parts, it is found that the decrease over time is predominantly due to a fall in the polar fraction, while the dispersive surface energy marginally decreases from approximately 32 to 28 mN/m.

The decrease in surface energy of vacuum coated films with time is a well known phenomenon within the metallizing and converting industries [27-29]. This ageing effect is believed to be due to the transfer of polymeric material (oligomers) and migratory additives from the reverse side of the coated film onto the coating, and also migration from the bulk polymer through the coating onto its surface via defects. BOPP film surfaces freshly coated with either aluminum or aluminum oxide exhibit a very high surface energy (several 100 mN/m) and are therefore extremely reactive. Consequently, the surface can attract low-energy mobile materials and contaminates quickly. This happens as soon as the film is wound into roll form after the coating process and the fresh coating surface is in direct contact with the polymer back surface. [30, 31]

XPS surface analysis of the AlO_x coated BOPP and PET films in this study confirmed the presence of carbon based material as well as film additives on the AlO_x coating, assumed to have come from contact with the reverse side of the film.

G. Acrylate top coat

A way of further enhancing the barrier properties of AlO_x coated films is to deposit an additional organic top coat, such as an acrylate coating, onto the AlO_x layer. Acrylate deposition can be achieved via flash evaporation of a monomer liquid in vacuum. These monomers condense as a liquid film on the surface to be coated and are subsequently radiation cured using ultraviolet light or electron beam technology in order to obtain a cross linked, solid layer [32]. In this study, an approximately 1 µm thick acrylate layer was deposited by Sigma Technologies via the process described above. Barrier results before and after acrylate deposition are summarized in *Table 5*.

Table 5 – Barrier performance of AlO_x coated BOPP films with and without acrylate top coat

Film	Description	OTR		WVTR	
		cm³/(m² d)	BIF	g/(m² d)	BIF
BOPP B	AlO_x	85.56 ± 16.80	-	5.89 ± 0.18	-
	AlO_x + acrylate	2.05 ± 0.44	42	3.88 ± 0.16	1.5
BOPP C	AlO_x	25.35 ± 1.38	-	4.73 ± 0.07	-
	AlO_x + acrylate	1.89 ± 0.31	13	0.40 ± 0.01	12

The results show that oxygen barrier as well as water barrier could be further improved down to levels around 2 cm³/(m² d) and below 1 g/(m² d) for commodity grade BOPP, respectively. The obtained barrier enhancement by the acrylate top coat is believed to be due to protection of the inorganic barrier layer from intense stress and damage based on the polymer coat's abrasion resistance and mechanical robustness, as mentioned by other researchers [33-36]. Furthermore, it is assumed that the acrylate fills up defects such as cracks, pinholes or grain boundaries in the AlO_x coating [16] (analogous to nanoparticles plugging defects as described by Ramadas et al. [37]), thus reducing the permeation coefficient within the defects from that of air to that of the acrylate. However, the reason for the big

difference in the moisture barrier obtained with acrylate for AlO_x coated BOPP B and C is so far unknown.

SUMMARY AND CONCLUSIONS

The barrier performance of packaging grade PET and BOPP films, coated with reactively evaporated aluminum oxide with a thickness of 9 to 11 nm, strongly depends on the surface properties of the plain film and the aluminum oxide film nucleation, growth and structure, which do not only vary to a large extend between the different polymer film types but can also change significantly within one substrate type. Whilst AlO_x coated PET films deliver consistent barrier results, BOPP reveals considerable variations, depending on the individual substrate. The general rule of thumb that a higher surface energy of the plain film results in better growth and, therefore greater barrier of the coated film, may well explain the differences in barrier levels between AlO_x coated PET and BOPP. However, in the case of the BOPP films, the surface energy itself was not a good indicator as all three standard BOPP films showed a similar level. Plain film surface defects such as the 'dimples' found on BOPP A appeared to be reproduced in the AlO_x coating, thus causing pores and impairing the oxygen barrier properties. The origin of these defects in the plain film surface needs to be further investigated. Another interesting finding is the surprisingly high AlO_x adhesion, which in all cases was higher than the intrinsic strength of the BOPP films. The use of a special skin layer on the plain BOPP film as well as the application of an acrylate top coat onto the AlO_x layer resulted in significant improvement of the barrier levels obtained.

ACKNOWLEDGEMENTS

The authors would like to thank Sigma Technologies Int'l, LLC (Tuscon AZ, USA) for depositing acrylate top coats as well as film producers and customers including Brückner Maschinenbau GmbH & Co.KG (Siegsdorf, Germany) for supplying base films. Additionally, we are grateful to Innovia Films Ltd. (Wigton, United Kingdom) for being able to use their analytical facilities, the Fraunhofer Institute for Process Engineering and Packaging IVV (Freising, Germany) for giving access to their AFM and Dr. Steve Hinder of the University of Surrey (Guildford, United Kingdom) for performing XPS analysis. Furthermore, we thankfully acknowledge Dr. Charles Bishop for his valued comments and input.

REFERENCES

1. *The future of transparent barrier films to 2011-*. 2004, Pira International Ltd.
2. Catalá, R. and R. Gavara, *Review: Alternative high barrier polymers for food packaging.* Food Science and Technology International, 1996. **2**(5): p. 281-291.
3. Yasuhara, A., T. Katami, and T. Shibamoto, *Formation of dioxins from combustion of polyvinylidene chloride in a well-controlled incinerator.* Chemosphere, 2006. **62**(11): p. 1899-1906.
4. Kelly, R.S.A., *Development of clear barrier films in Europe.* 36th Annual Technical Conference Proceedings, Society of Vacuum Coaters, 1993: p. 312-316.
5. Kelly, R.S.A., *Development of aluminium oxide clear barrier films.* 37th Annual Technical Conference Proceedings, Society of Vacuum Coaters, 1994: p. 144-148.
6. Schiller, S., et al., *How to produce Al_2O_3 coatings on plastic films.* Proceedings of 7th International Conference on Vacuum Web Coating, 1993: p. 194-219.
7. Schiller, S., et al., *Plasma-activated high-rate deposition of oxides on plastic films.* 37th Annual Technical Conference Proceedings, Society of Vacuum Coaters, 1994: p. 203-210.
8. Schiller, N., et al., *Innovative clear barrier technology for the packaging industry.* AIMCAL Fall Technical Conference, 2008.
9. Günther, S., et al., *Innovative transparent barrier for packaging.* 52nd Annual Technical Conference Proceedings, Society of Vacuum Coaters, 2009: p. 727-729.

10. Bichler, C., et al., *Adhesion mechanism of aluminum, aluminum oxide, and silicon oxide on biaxially oriented polypropylene (BOPP), poly(ethyleneterephthalate) (PET), and poly(vinyl chloride) (PVC).* Journal of Adhesion Science and Technology, 1997. **11**(2): p. 233-246.
11. Langowski, H.-C., *Surface Modification of Polymer Films for Improved Adhesion of Deposited Metal Layers.* Journal of Adhesion Science and Technology, 2011. **25**(1-3): p. 223-243.
12. Owens, D.K. and R.C. Wendt, *Estimation of the surface free energy of polymers.* Journal of Applied Polymer Science, 1969. **13**(8): p. 1741-1747.
13. Rabel, W., *Einige Aspekte der Benetzungstheorie und ihre Anwendung auf die Untersuchung und Veränderung der Oberflächeneigenschaften von Polymeren.* Farbe und Lack, 1971. **77**(10): p. 997-1005.
14. Kaelble, D.H., *Dispersion-Polar Surface Tension Properties of Organic Solids.* The Journal of Adhesion, 1970. **2**(2): p. 66 - 81.
15. Decker, W. and B. Henry, *Basic Principles of Thin Film Barrier Coatings.* 45th Annual Technical Conference Proceedings, Society of Vacuum Coaters, 2002: p. 492-502.
16. Miesbauer, O., M. Schmidt, and H.-C. Langowski, *Stofftransport durch Schichtsysteme aus Polymeren und dünnen anorganischen Schichten (Mass transport through layer systems consisting of polymers and thin inorganic coatings).* Vakuum in Forschung und Praxis, 2008. **20**(6): p. 32-40.
17. Hanika, M., H.-C. Langowski, and W. Peukert, *Simulation and Verification of Defect-Dominated Permeation Mechanisms in Multiple Structures of Inorganic and Polymeric Barrier Layers.* 46th Annual Technical Conference Proceedings, Society of Vacuum Coaters, 2003: p. 592-599.
18. Erlat, A.G., et al., *Mechanism of Water Vapor Transport through PET/AlOxNy Gas Barrier Films.* The Journal of Physical Chemistry B, 2004. **108**(3): p. 883-890.
19. Tropsha, Y.G. and N.G. Harvey, *Activated Rate Theory Treatment of Oxygen and Water Transport through Silicon Oxide/Poly(ethylene terephthalate) Composite Barrier Structures.* The Journal of Physical Chemistry B, 1997. **101**(13): p. 2259-2266.
20. Kromminga, T. and G. Van Esche, *Anti-blocking Additives*, in *Plastic Additives Handbook*, H. Zweifel, R.D. Maier, and M. Schiller, Editors. 2008, Carl Hanser Verlag: Munich. p. 613-628.
21. Benmalek, M. and H.M. Dunlop, *Inorganic coatings on polymers.* Surface and Coatings Technology, 1995. **76-77**(Part 2): p. 821-826.
22. Deng, C.S., et al., *Nucleation and growth of gas barrier aluminium oxide on surfaces of poly(ethylene terephthalate) and polypropylene: effects of the polymer surface properties.* Journal of Polymer Science Part B: Polymer Physics, 2000. **38**(23): p. 3151-3162.
23. Low, H. and Y. Xu, *Moisture barrier of AlxOy coating on poly(ethylene terephthalate), poly(ethylene naphthalate) and poly(carbonate) substrates.* Applied Surface Science, 2005. **250**(1-4): p. 135-145.
24. Henry, B.M., et al., *Gas barrier properties of transparent metal oxide coatings on PET film.* 47th Annual Technical Conference Proceedings, Society of Vacuum Coaters, 2004: p. 609-614.
25. McClure, D.J. and N. Copeland, *Evaporated aluminum on polyester: optical, electrical, and barrier properties as a function of thickness and time (Part II).* AIMCAL Fall Technical Conference, 2010.
26. Mittal, K.L., *Adhesion measurements of films and coatings: a commentary*, in *Adhesion Measurements of Films and Coatings*, K.L. Mittal, Editor. 1995, VSP: Utrecht. p. 1-13.
27. Bishop, C.A., *Question re. decline in metal coating surface energy*. 2010: http://www.convertingquarterly.com/blogs/vacuum-web-coating/id/1588/question-re-decline-in-metal-coating-surface-energy.aspx [access: 09.08.2011].
28. Mount, E., *Aluminium layer contamination in wound rolls of metallized films*. 2010: http://www.convertingquarterly.com/blogs/substrate-secrets/id/2190/aluminum-layer-contamination-in-wound-rolls-of-metallized-films.aspx [access: 09.08.2011].
29. Mount, E., *PET film coatings for maintaining the surface energy of the films*. 2011: http://www.convertingquarterly.com/blogs/substrate-secrets/id/2661/pet-film-coatings-for-maintaining-the-surface-energy-of-the-films.aspx [access: 09.08.2011].
30. Marra, J.V., *Metallized Opp Film, Surface Characteristics and Physical Properties.* Journal of Plastic Film and Sheeting, 1988. **4**(1): p. 27-34.
31. Bishop, C.A., *Roll-to-roll vacuum deposition of barrier coatings*. 2010: Scrivener Publishing and John Wiley & Sons. 59-64.
32. Gross, M.E. and P.M. Martin, *Chapter 11: Vacuum Polymer Deposition*, in *Handbook of Deposition Technologies for Films and Coatings*, P.M. Martin, Editor. 2010, Elsevier. p. 532-553.
33. Affinito, J.D., et al., *A new method for fabricating transparent barrier layers.* Thin Solid Films, 1996. **290–291**(0): p. 63-67.
34. Affinito, J.D., et al., *PML/oxide/PML barrier layer performance differences arising from use of UV or electron beam polymerization of the PML layers.* Thin Solid Films, 1997. **308–309**(0): p. 19-25.
35. Miyamoto, T., et al., *Gas Barrier Performances of Organic-Inorganic Multilayered Films.* 44th Annual Technical Conference Proceedings, Society of Vacuum Coaters, 2001: p. 166-171.
36. Lewis, J.S. and M.S. Weaver, *Thin-film permeation-barrier technology for flexible organic light-emitting devices.* IEEE Journal of Selected Topics in Quantum Electronics, 2004. **10**(1): p. 45-57.
37. Ramadas, S., et al., *Nanoparticulate Barrier Films and Gas Permeation Measurement Techniques for Thin Film Solar and Display Applications.* AIMCAL Fall Technical Conference, 2008.